PCCP

PAPER

View Article Online
View Journal | View Issue

Cite this: *Phys. Chem. Chem. Phys.*, 2025, **27**, 12532

Viscosity prediction of CO_2-saturated imidazolium-based ionic liquids using the ε*-modified Sanchez–Lacombe equation of state and free volume theory with a new correction term†

Ryohei Otani, Yuya Hiraga * and Masaru Watanabe *

Received 26th March 2025,
Accepted 17th May 2025

DOI: 10.1039/d5cp01170a

rsc.li/pccp

Ionic liquids (ILs) have gained attention as solvents for carbon dioxide (CO_2) separation and as catalysts for CO_2 fixation. Viscosity is a fundamental transport property of ILs because it plays a significant role in their process efficiency. In this study, a viscosity prediction model for CO_2-saturated ILs was developed by combining the ε*-modified Sanchez–Lacombe equation of state (ε*-mod SL-EoS) and free volume theory (FVT) with a new correction term, $\beta x'$, where β and x' are the correction factor and molar ratio of CO_2 to IL, respectively. The viscosities were predicted by incorporating the mixture density, calculated using the ε*-mod SL-EoS, into the FVT, and the parameters for ε*-mod SL-EoS and FVT were calculated by correlating the high-pressure densities and viscosities of the ILs. Although the initial deviations, which are due to the affinity between ILs and CO_2, were considerable for the five imidazolium-based ILs studied in this work, they were improved by introducing $\beta x'$. β could be calculated using the solubility parameters of the ILs and CO_2, without requiring correlation. The average absolute relative deviations were 6.05–35.3% in the range of $x' < 1.0$, sufficiently predicting the viscosity of the IL + CO_2 mixtures.

1. Introduction

The development and application of carbon capture utilization and storage (CCUS) technology are expected to achieve carbon neutrality through the establishment of a carbon recycling industry. In this context, ionic liquids (ILs) have attracted attention not only as efficient solvents for CO_2 separation and capture but also as catalysts for CO_2 fixation.[1–4] In developing such CCUS technology, knowledge of fundamental physical properties is essential. Many researchers have extensively studied properties such as density,[5] viscosity,[6] and gas solubility[7] from both experimental and theoretical perspectives.

Among the fundamental physical properties, viscosity is a particularly important transport property because it significantly affects CO_2 diffusion and heat-transfer rates. CO_2 has been utilized in various processes to reduce the viscosity of IL solutions, and its effectiveness has been demonstrated.[8,9] For example, in CCUS-related research, the viscosity of ILs under CO_2 dissolution has often been investigated as an important physical property when selecting IL species for use in membrane separation or absorbents.[10–15] In addition, in CO_2-fixation reactions, improved reaction yields have been observed under high-pressure conditions,[16] and both the increased amount of dissolved CO_2 and the reduced solution viscosity have been considered to be contributing factors.[17] Owing to the numerous IL types, measuring the viscosities of all IL + CO_2 mixtures is difficult; therefore, a prediction model for viscosity must be developed.

Although many viscosity models have been reported for pure ILs,[6,11,18,19] those for IL + CO_2 mixtures are even rarer in the literature. Models based on free volume theory (FVT)[20] and friction theory (FT)[21] have been applied to predict the viscosity of IL + CO_2 mixtures as a theoretical model development approach. For each case, combining suitable equations of state is necessary to estimate the force or distance between the molecules; this is a repulsive/attractive force in FT and the density in FVT. For example, Shen *et al.*[22] combined FVT and FT with ePC-SAFT (electrolyte perturbed-chain statistical associating fluid theory)[23] and concluded that the average relative deviations (ARDs) for the correlation of the viscosities of an IL + CO_2 mixture were 15.8–32.3% for FVT and 4.14–20.0% for FT, respectively. On the other hand, Lopes *et al.*[24] proposed applying an empirical model to the viscosity of IL + CO_2 mixtures, and they achieved ARDs of 4.4–13% for viscosity correlation. Although these models can correlate the viscosities of IL + CO_2 mixtures with sufficiently high accuracy, they

Research Center of Supercritical Fluid Technology, Tohoku University, Aramaki Aza Aoba 6-6-11, Aoba-ku, Sendai, Miyagi 980-8579, Japan.
E-mail: yuya.hiraga.d6@tohoku.ac.jp, masaru.watanabe.e2@tohoku.ac.jp

† Electronic supplementary information (ESI) available. See DOI: https://doi.org/10.1039/d5cp01170a

require experimental data for parameter determination. Specifically, the model proposed by Shen *et al.*[22] requires the determination of binary adjustable parameters, whereas the model developed by Lopes *et al.*[24] involves fitting polynomial coefficients. Both approaches require a correlation with experimental measurements.

In this study, FVT was used to calculate viscosity, η. Doolittle[20] used the occupied volume, V_0; free volume, V_f; and substantial constants A and B to express viscosity as follows:

$$\ln \eta = \ln A + B\left(\frac{V_0}{V_f}\right) \quad (1)$$

Using the specific volume (V) and V_f, the free volume ratio, f, can be expressed as follows:

$$V_f = V - V_0 \quad (2)$$

$$f = \frac{V - V_0}{V} = \frac{V_f}{V} \quad (3)$$

If V_0 is large, $V_0 \gg V_f$ is assumed. Therefore, from eqn (1)–(3), the viscosity can be expressed using eqn (4), inserting constants A and B as well as f.

$$\ln \eta = \ln A + \left(\frac{B}{f}\right) \quad (4)$$

The ε^*-modified Sanchez–Lacombe equation of state (ε^*-mod SL-EoS)[25–27] was selected in this study to calculate the free volume ratio. Various methods exist for determining the free volume, including molecular dynamics[28–31] simulations and experimental approaches.[32–35] However, one of the practical and theoretically well-founded methods is the use of an appropriate equation of state. ε^*-mod SL-EoS[25] is one of the lattice fluid type equations of state and can be expressed as follows:

$$\tilde{\rho}^2 + \tilde{P} + \tilde{T}\left[\ln(1-\tilde{\rho}) + \left(1 - \frac{1}{r}\right)\tilde{\rho}\right] = 0 \quad (5)$$

$$\varepsilon^*(T) = \varepsilon_0 \frac{T}{1/\alpha + T} \quad (6)$$

$$\rho^* = \frac{M_w}{r v^*} \; P^* = \frac{\varepsilon^*(T)}{v^*} \; T^* = \frac{\varepsilon^*(T)}{R} \quad (7)$$

$$\tilde{\rho} = \frac{\rho}{\rho^*} \; \tilde{P} = \frac{P}{P^*} \; \tilde{T} = \frac{T}{T^*} \quad (8)$$

where T^*, P^*, ρ^*, v^* and ε^* are the characteristic parameters for temperature, pressure, density, volume, and interaction energy, respectively. Similarly, T, P, ρ, r, ε_0, and α are the temperature, pressure, density, the number of lattice sites occupied by one molecule, the asymptotic value of the interaction energy, and the temperature-dependent parameter, respectively; M_w and R are the molar mass and gas constant, respectively. The lattice fluid theory was originally applicable to high-density solutions such as polymer solutions. However, ILs exhibit polymer-like high-density characteristics owing to Coulombic interactions. Therefore, theories such as the SL-EoS and the ε^*-mod SL-EoS have been applied to ILs. As a representative example, our research has demonstrated that this equation could accurately correlate and predict the densities of various pure ILs over a wide temperature range and at pressures up to 200 MPa.[25,36–38] For IL + CO_2 mixtures, the ε^*-mod SL-EoS successfully predicted the swelling ratio of ILs caused by dissolving CO_2.[39] These results indicate that the ε^*-mod SL-EoS is capable of accurately representing not only the pure component density of ILs but also the density of IL + CO_2 mixtures. Lattice-fluid theory is related to FVT, allowing f to be expressed as $1 - \tilde{\rho}$, where $\tilde{\rho}$ represents the reduced density in the lattice-fluid theory.[40] From the perspective of correlation accuracy for density, other candidate equations of state, such as ePC-SAFT, exist.[41,42]

However, the equations of state based on these lattice fluid theories can be directly incorporated into the free volume ratio in FVT. These approaches are expected to facilitate the development of viscosity prediction models for IL + CO_2 mixtures.

In this study, an FVT model incorporating the ε^*-mod SL-EOS was developed to predict the viscosities of IL + CO_2 mixtures. The model was applied to the viscosities of five imidazolium-based IL + CO_2 mixtures, for which viscosity measurements under CO_2-saturated conditions have been reported (Table 1). The aim was to predict the viscosity of IL + CO_2 mixtures without correlating it with the experimental viscosity data by applying the ε^*-mod SL-EOS, which is expected to accurately represent the free volume. This approach was expected to avoid the use of binary adjustable parameters or enable their estimation from other physical constants, thus eliminating the need for correlation with the experimental viscosity data.

2. Model

2.1 Overall concept for viscosity calculation by FVT with ε^*-mod SL-EoS

In this study, the viscosities were calculated using the procedure shown in Fig. 1. The reduced density of ILs, $\tilde{\rho}_{IL}$, was calculated using ε^*-mod SL-EoS, and the free volume ratio for the pure IL, f_{IL}, was replaced by $1 - \tilde{\rho}_{IL}$. In the case of IL + CO_2 mixtures, the reduced density of the mixtures ($\tilde{\rho}_{mix}$) was used. Then, A and B were determined by correlating them with the viscosity of the pure ILs. Because A and B were observed to be temperature dependent, the temperature dependence was expressed as $A(T)$ and $B(T)$. The viscosities of the mixtures were

Table 1 Viscosity of IL + CO_2 mixtures under CO_2 saturated conditions

Name	Temperature [K]	Pressure [MPa]	Ref.
[emim][Tf_2N]	298.15–343.15	0.1–29	43
	323.15	1–9	44
[hmim][Tf_2N]	298.15–343.15	0.1–29	43
	278.15–303.15	0.1	45
[dmim][Tf_2N]	298.15–343.15	2–13	43
[emim][FAP]	303.15–343.15	1–10	44
[hmim][FAP]	303.15–343.15	1–10	44

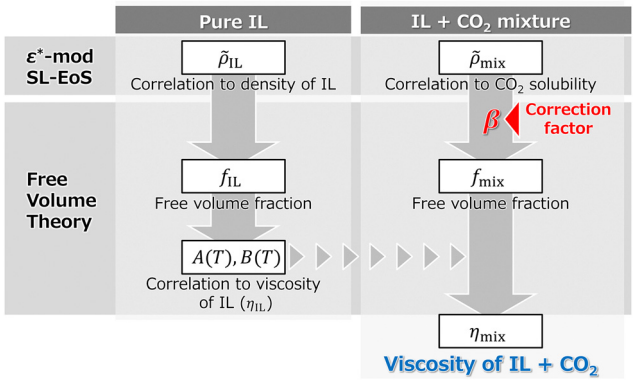

Fig. 1 Flow diagram of the viscosity calculations in this study.

calculated using eqn (9).

$$\ln \eta_{mix} = \ln A(T) + \left(\frac{B(T)}{(1-\tilde{\rho}_{mix}) + \beta x'}\right) \quad (9)$$

In addition, the correction factor, β, was introduced for the FVT in this study. Because cation–anion interactions have significant effects on viscosity,[46,47] viscosity changes in IL + CO_2 mixtures cannot be fully explained only by changes in the free volume. To accurately express the viscosity, the correction term, $\beta x'$, was introduced into the free volume term using β and the molar ratio of CO_2 to IL, x', as shown in eqn (10). The molar ratio of CO_2 to IL has been used to describe the reaction between chemically absorbent ILs and CO_2[48–50] as well as the relationship between the Raman spectra and CO_2 solubility.[51] In this study, x' is used to represent the effect of CO_2 on one mole of IL, where x' and the modified free volume ratio are expressed as follows:

$$x' = \frac{n_{CO_2}}{n_{IL}} = \frac{x}{1-x} \quad (10)$$

$$f_{mix} = (1 - \tilde{\rho}_{mix}) + \beta x' \quad (11)$$

where n_{CO_2} and n_{IL} are the moles of CO_2 and the IL, respectively. The CO_2 solubility, x, was calculated using ε*-mod SL-EoS and x' was a simple unit conversion of x.

2.2 Pure IL systems

Four pure component parameters (ε_0, v*, α, r), eqn (5)–(8) are required to calculate the ε*-mod SL-EoS. These parameters were determined by correlating them with the densities of pure ILs reported in the literature and minimizing the average relative deviation (ARD), as defined in eqn (12).

$$ARD = \frac{100}{n}\sum_{i=1}^{n}\left|\frac{\rho_{IL,cal} - \rho_{IL,exp}}{\rho_{IL,exp}}\right| \quad (12)$$

where $\rho_{IL,cal}$ and $\rho_{IL,exp}$ are the calculated and experimental densities of pure ILs, respectively; and n is the number of data points. Using the determined four pure component parameters, $\tilde{\rho}_{IL}$ was calculated, and then η_{IL} was calculated using eqn (13). The temperature dependences of $A(T)$ and $B(T)$ were accounted for, as expressed in eqn (14), and the parameters a_1, a_2, b_1, and b_2 were determined by correlating them with the viscosities of the ILs reported in the literature. The ARD defined in eqn (15) was used as the objective function for the correlation.

$$\ln \eta_{IL} = \ln A(T) + \left(\frac{B(T)}{1-\tilde{\rho}_{IL}}\right) \quad (13)$$

$$A(T) = a_1 T^{a_2} \quad B(T) = b_1 T^{b_2} \quad (14)$$

$$ARD = \frac{100}{n}\sum_{i=1}^{n}\left|\frac{\eta_{IL,cal} - \eta_{IL,exp}}{\eta_{IL,exp}}\right| \quad (15)$$

where $\eta_{IL,cal}$ and $\eta_{IL,exp}$ are the calculated and experimental viscosities of the pure ILs, respectively.

2.3 IL + CO_2 binary systems

For the IL + CO_2 mixture calculation using the ε*-mod SL-EoS, the following mixing rules were applied:

$$P^* = \sum_{i=1}^{2}\varphi_i P_i^* - \frac{1}{2}\sum_{i=1}^{2}\sum_{j=1}^{2}\varphi_i\varphi_j\Delta P_{i,j}^* \quad (16)$$

$$\Delta P_{i,j}^* = P_i^* + P_j^* - 2(1-k_{i,j})\cdot\sqrt{P_i^* P_j^*} \quad (17)$$

$$k_{i,j} = k_{j,i} = k_c + k_T T \quad (18)$$

where k_{ij} is the interaction parameter between substances i and j, expressed as a linear equation with temperature dependence using intercept k_c and slope k_T, as shown in eqn (18); and φ_i and φ_j represent the volume fractions of components i and j, respectively. For the phase equilibrium calculations, the ILs were assumed to be insoluble in the CO_2 vapor phase. The interaction parameters were determined by correlating them with the CO_2 solubility reported in the literature, minimizing the ARD in the following equation:

$$ARD = \frac{100}{n}\sum_{i=1}^{n}\left|\frac{x_{CO_2,cal} - x_{CO_2,exp}}{x_{CO_2,exp}}\right| \quad (19)$$

where $x_{CO_2,cal}$ and $x_{CO_2,exp}$ are the calculated and experimental solubilities of CO_2 in the IL, respectively. Other parameters (ε_{mix}^*, r_{mix}, v_{mix}^*, and $\tilde{\rho}_{mix}$) were calculated based on their definitions.[25] The reduced density in the mixtures, $\tilde{\rho}_{mix}$, was calculated during the process of calculating $x_{CO_2,calc}$.

3. Results and discussion

3.1 Pure-component parameters for the ε*-mod SL-EoS determined by correlation with pure IL density

Fig. 2 shows the correlation results for the density of pure [emim][Tf_2N],[52] and those for other pure ILs[53–63] are presented in Fig. S1–S4 (ESI†). The parameters in the ε*-mod SL-EoS (eqn (5)–(8)) and their ARD values calculated using eqn (12) are summarized in Table 2. The ARD values for the densities of the five pure ILs ranged from 0.048% to 0.20%. Using the ε*-mod SL-EoS enabled accurate correlation of the pure IL densities over a wide range of temperatures and pressures.

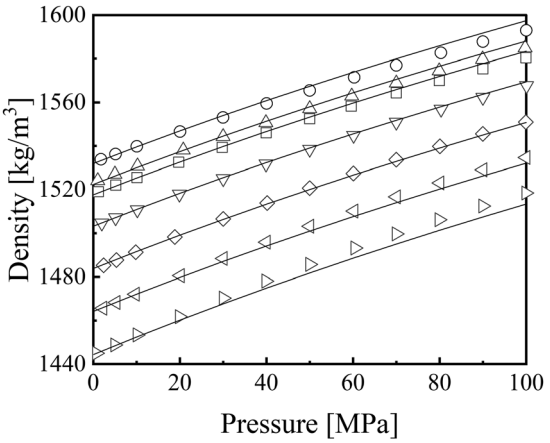

Fig. 2 Correlation results for the density of [emim][Tf_2N].[52] Symbols: ○, 283 K; Δ, 293 K; □, 313 K; ▽, 323 K; ◊, 333 K; ◁, 353 K; ▷, 373 K. Lines: ε*-mod SL-EoS.

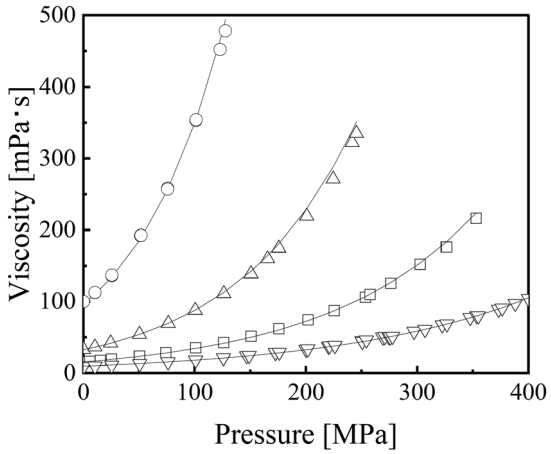

Fig. 3 Correlation results for viscosity of [emim][Tf_2N].[65] Symbols: ○, 273.15 K; Δ, 298.15 K; □, 323.15 K; ▽, 348.15 K. Lines: FVT + ε*-mod SL-EoS.

3.2 FVT parameters determined by correlation with pure IL viscosity

Fig. 3 shows the correlation results for the viscosity of pure [emim][Tf_2N],[65] and the viscosities of other pure ILs[44,57,58,60,66–69] are shown in Fig. S5–S8 (ESI†). The parameters a_1, a_2, b_1, and b_2 in eqn (14) and the ARD values obtained using eqn (15) are listed in Table 3: the ARD values of the viscosities of the five pure ILs ranged from 1.6% to 5.1%. The viscosities of the pure ILs were successfully correlated across a wide pressure range using the FVT + ε*-mod SL-EoS model.

3.3 Densities of IL + CO_2 mixtures and interaction parameters of ε*-mod SL-EoS determined by correlation with CO_2 solubility

Fig. 4 shows the correlation results for CO_2 solubility in [emim][Tf_2N],[44,71,72] and those for other ILs[57,73–82] are presented in Fig. S9–S12 (ESI†). Table 4 lists the interaction parameters, k_c and k_T, in eqn (18) and their ARD values using eqn (19). The ARD values for CO_2 solubility in the five ILs ranged from 1.5% to 5.4%, which indicates a sufficiently accurate correlation when considering the uncertainties and variations in the literature values.

Fig. 5 shows the mixed density, ρ_{mix}, of the [emim][Tf_2N] + CO_2 mixture[72] predicted by eqn (5)–(8).

For the other IL + CO_2 mixture systems, the densities were not compared owing to a lack of literature data. The ARD for ρ_{mix} (eqn 20) was 0.59%, demonstrating that the proposed method enables accurate prediction of the mixture density when considering their reported uncertainty (0.7%).[72]

$$\mathrm{ARD} = \frac{100}{n}\sum_{i=1}^{n}\left|\frac{\rho_{\mathrm{mix,cal}} - \rho_{\mathrm{mix,exp}}}{\rho_{\mathrm{mix,exp}}}\right| \qquad (20)$$

3.4 Viscosity of IL + CO_2 mixtures

Fig. 6 shows the viscosities, η_{mix}, of the [emim][Tf_2N] + CO_2 mixture;[43,44] those for other IL + CO_2 mixtures[43–45] are presented in Fig. S13–S16 of the ESI.† The viscosity of [bmim][PF_6] + CO_2 has also been reported,[83] but discrepancies in the viscosity trends of this system have been pointed out in another study.[84] For this reason, it was excluded from the scope of this investigation. As shown in the prediction using $\beta = 0$ in Table 5, the ARD values for each system using eqn (21) were considerable for all IL + CO_2 mixtures. One reason for this deviation is that the decrease in density observed for the IL + CO_2 mixtures, as described in Section 3.3, is smaller than the decrease in viscosity. According to eqn (9), the density changes directly influence the viscosity, indicating that the trends coincide. However, the viscosity decreased sharply, whereas the density decreased gradually, with increasing CO_2 mole fraction in the system. The model was generally sufficient to describe the behavior of IL + CO_2 mixtures. However, expressing their viscosity only in terms of the density change, that is, the change

Table 2 Pure-component parameters for ε*-mod SL-EoS and ARDs

Name	M_w [g mol^{-1}]	ε_0 [J mol^{-1}]	v* [cm^3 mol^{-1}]	1/α [−]	r [−]	ARD [%]	Ref.
[emim][Tf_2N]	391.3	9982.8	1.205	762.6	159.7	0.095	52 and 64
[hmim][Tf_2N]	447.4	11 989	0.9604	1070	241.6	0.20	53–55
[dmim][Tf_2N]	503.5	10 165	1.019	873.4	272.5	0.070	56
[emim][FAP]	556.2	5872	6.929	99.79	42.41	0.048	57–62
[hmim][FAP]	612.3	5520	9.452	38.17	57.75	0.053	57, 62 and 63
CO_2	44.01	3060	3.512	7.762	79.34	—	25[a]

[a] Parameters obtained from ref. 25.

Table 3 Parameters a_1, a_2, b_1, and b_2 for FVT + ε*-mod SL-EoS (eqn (13) and (14)) and ARDs

Name	a_1	a_2	b_1	b_2	ARD [%]	Ref.
[emim][Tf_2N]	2.290×10^{-17}	6.144	9.176×10^{4}	−1.910	2.9	65 and 70
[hmim][Tf_2N]	4.736×10^{-10}	2.983	6.494×10^{3}	−1.378	5.1	58, 60, 66 and 67
[dmim][Tf_2N]	9.896×10^{4}	−2.687	2.175×10^{2}	−0.7838	2.3	68
[emim][FAP]	2.003×10^{7}	−2.693	1.863×10^{4}	−1.964	1.6	44, 57, 58, 60 and 69
[hmim][FAP]	5.149×10^{6}	−2.436	2.189×10^{5}	−2.400	3.0	44, 58, 63 and 69

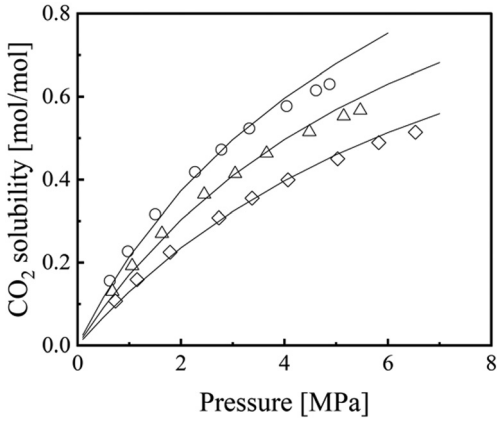

Fig. 4 Correlation results for CO_2 solubility in [emim][Tf_2N].[72] Symbols: ○, 298.15 K; Δ, 313.15 K; ◊, 333.15 K.[72] Lines: ε*-mod SL-EoS.

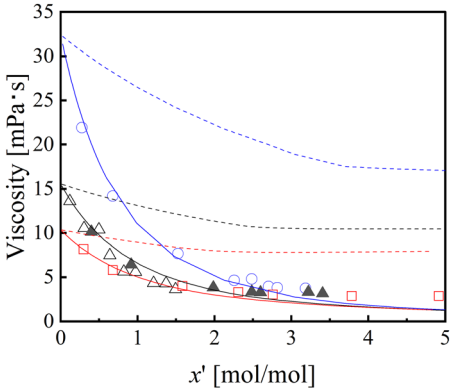

Fig. 6 Prediction and correlation results for the viscosity of the [emim][Tf_2N] + CO_2 mixture. Symbols: ○, 298.15 K;[43] Δ, 323.15 K;[43] □, 343.15 K;[43] ▲, 323.15 K.[44] Dashed lines: prediction with FVT + ε*-mod SL-EoS (β = 0). Solid lines: correlation with FVT + ε*-mod SL-EoS ($\beta \neq 0$).

Table 4 Interaction parameters of IL + CO_2 for ε*-mod SL-EoS with ARDs calculated using eqn (20)

Name	$k_C \times 10^2$	$k_T \times 10^4$	ARD [%]	Ref.
[emim][Tf_2N]	−3.204	−4.127	4.5	44, 71 and 72
[hmim][Tf_2N]	−2.904	−5.976	4.0	57 and 73–76
[dmim][Tf_2N]	1.281	−6.428	1.5	73 and 77
[emim][FAP]	−3.701	1.451	5.4	57 and 78–80
[hmim][FAP]	−3.092	0.8253	4.6	57 and 80–82

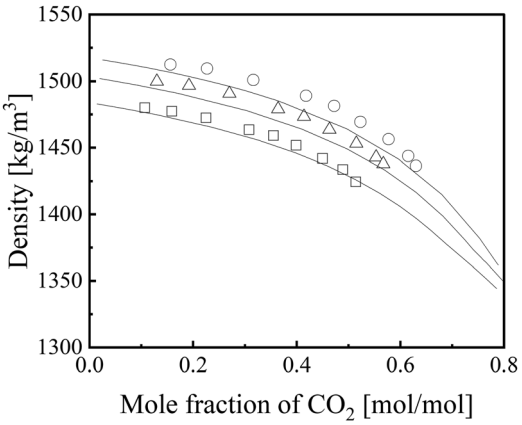

Fig. 5 Prediction results for density of [emim][Tf_2N] + CO_2.[72] Symbols: ○, 298.15 K; Δ, 313.15 K; □, 333.15 K. Lines: ε*-mod SL-EoS.

Table 5 ARDs of the prediction and correlation results of the viscosities of the IL + CO_2 mixtures

	Prediction (β = 0)	Correlation ($\beta \neq 0$)		
Name	ARD [%]	β	ARD [%]	Ref.
[emim][Tf_2N]	180	0.04023	15.6	43 and 44
[hmim][Tf_2N]	188	0.02899	17.2	43 and 45
[dmim][Tf_2N]	412	0.02499	10.3	43
[emim][FAP]	173	0.1080	14.7[a]	44
[hmim][FAP]	136	0.1096	12.4[a]	44
Overall	215		14.3	

[a] Molar ratio, x', less than 0.1.

in the free volume ratio owing to CO_2 saturation, is still challenging. Therefore, the model must be modified to account for the observed viscosity reduction.

$$\mathrm{ARD} = \frac{100}{n}\sum_{i=1}^{n}\left|\frac{\eta_{\mathrm{mix,cal}} - \eta_{\mathrm{mix,exp}}}{\eta_{\mathrm{mix,exp}}}\right| \quad (21)$$

3.4.1 Correction factor determined by correlation with IL + CO_2 viscosity. The correction factor, β, was determined by correlating the viscosity of the IL + CO_2 mixtures, η_{mix}, to minimize the ARD defined in eqn (21). Discontinuities were observed in the experimental data for the [emim][FAP] + CO_2 and [hmim][FAP] + CO_2 mixtures.

In high-solubility regions, such as [bmim][PF_6] + CO_2 mixtures, the aggregation structure of ILs might be disrupted.[85] Therefore, the correlation was limited to the region where the molar ratio of CO_2 to the IL, x', was less than 1.0. These correlation results are also shown in Table 5 along with the determined β values and ARD values. The overall deviation was improved from 215% to 14.3% by introducing the correlation using β. The solid lines in Fig. 6 and Fig. S13–S16 (ESI†) represent the viscosities of the IL + CO_2 mixtures, η_{mix}, calculated after introducing the correction term, $\beta x'$.

Previously, Shen *et al.*[22] applied models combining ePC-SAFT with either FVT or FT to the literature-reported viscosities of the [hmim][Tf_2N] + CO_2 system.[43] The reported ARD was 32.31% for the FVT + ePC-SAFT model and 10.22% for the FT + ePC-SAFT model. By comparison, the FVT + ε*-mod SL-EoS model proposed in the present study yielded an ARD of 17.0%, demonstrating better accuracy than the FVT + ePC-SAFT model, although slightly lower than that of the FT + ePC-SAFT model. Similarly, Lopes *et al.*[24] used a polynomial-type equation to correlate the literature values of the viscosities of IL + CO_2 systems for [hmim][Tf_2N][43] and [dmim][Tf_2N],[43] achieving correlation accuracies of 25.0% and 18.9%, respectively. Comparing these with the values obtained in this study (*i.e.*, 17.0% and 10.3%, respectively), our model demonstrated superior performance. For the [emim][Tf_2N] + CO_2 mixtures, the introduction of $\beta x'$ reduced the ARD to 15.6%. The parity plot (Fig. 7) shows that the model demonstrated good correlation, particularly in the regions where the viscosity exceeded 10 mPa s. However, a larger deviation was observed in the low-viscosity regions below 10 mPa s. Based on the β value, no clear trend was observed with respect to the cation side-chain length, but the difference in anion species was significant. Specifically, ILs containing the [FAP] anion require a larger correction than those comprising [Tf_2N] anions, indicating that the contribution of the [FAP] anion to their viscosity cannot be fully explained by the free volume alone.

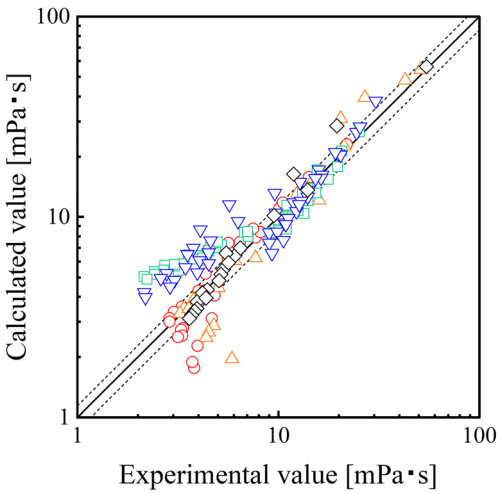

Fig. 7 Parity plot for the viscosity of the IL + CO_2 mixture. Symbols: ○, [emim][Tf_2N] + CO_2 mixture;[43] △, [hmim][Tf_2N] + CO_2 mixture;[43] ◊, [dmim][Tf_2N] + CO_2 mixture;[43] ▽, [emim][FAP] + CO_2 mixture;[44] ▽, [hmim][FAP] + CO_2 mixture.[44] Dashed lines: overall ARDs (14.3%; see Table 5) of the FVT + ε*-mod SL-EoS model.

Fig. 8 shows a schematic depicting the physical meaning of the free volume (*i.e.*, the distance between molecules) and the correction factor for the viscosity reduction caused by CO_2 dissolution. CO_2 dissolution in ILs has been proposed to be caused by the voids within the IL, as reported in several studies.[28–30,86] On the other hand, the expansion of the IL volume owing to CO_2 dissolution, that is, the expansion of the free volume, is not large but rather limited to slight structural changes.[87–91]

This indicates that the viscosity decrease accompanying CO_2 dissolution in ILs is not merely due to an increase in the free volume but also partially results from newly formed interactions between CO_2 and the ions of the IL (particularly its anion), which weakens the attractive forces between the cation and anion of the IL. The reduction in ionic interactions has been demonstrated through molecular dynamics calculations.[90,91] Therefore, the $\beta x'$ term introduced in this study can be considered to account for the interaction changes that are not fully captured by the FVT-based model.

3.4.2 Correction factor predicted by solubility parameters. To predict β, the solubility parameters of CO_2 and the ILs were used. Substances with similar solubility parameters tend to dissolve well and exhibit good affinity, and the influence of the difference in solubility parameters between ILs and CO_2 on CO_2 solubility has been reported.[92,93] Meanwhile, several approaches use the differences in solubility parameters between solvents and solutes to predict correction factors in phase equilibrium modelling.[94–97] Referring to these studies, the following formulation was established:

$$\beta = \frac{1}{|\delta_{IL} - \delta_{CO_2}|} \quad (22)$$

The details of the calculation method for determining solubility parameters are provided in the ESI,† and previous paper.[98] β is predicted by taking the reciprocal of the difference between δ_{IL} and δ_{CO2} as molecules with higher affinity were assumed to have larger correction factors.

Fig. 9 shows the contributions of $1 - \tilde{\rho}_{mix}$ (dashed lines) and $\beta x'$ (solid lines) to the viscosity of [emim][Tf_2N] + CO_2 and [emim][FAP] + CO_2 mixtures. The results for the other mixtures are shown in Fig. S17–S19 (ESI†). The contribution of $\beta x'$ was larger in FAP-based IL + CO_2 mixtures than in [Tf_2N]-based mixtures. This is attributed to the fluorine content in the [FAP] anion, which induces a strong dipole interaction with CO_2 molecules, enhancing their affinity.[91] In other words, the tendency of the β values of the ILs consisting of the [FAP] anion to be larger and thus require a greater correction (Table 5) was successfully represented by eqn (22). Therefore, the correction term, $\beta x'$, which is one of the factors contributing to the viscosity reduction shown in Fig. 9, represents the contribution of the weakened cation–anion interactions in the IL owing to CO_2 dissolution. Fig. S20–S24 (ESI†) present the viscosities of the predicted β values obtained using this method, and Fig. 10 shows the parity plot. For all IL + CO_2

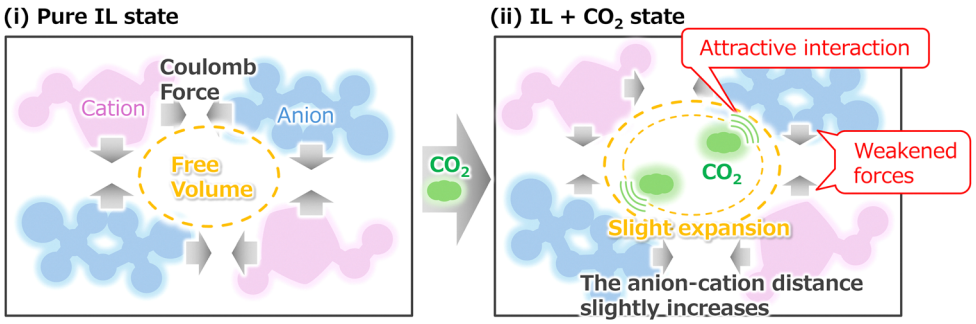

Fig. 8 The mechanism of viscosity reduction caused by CO_2 dissolution.

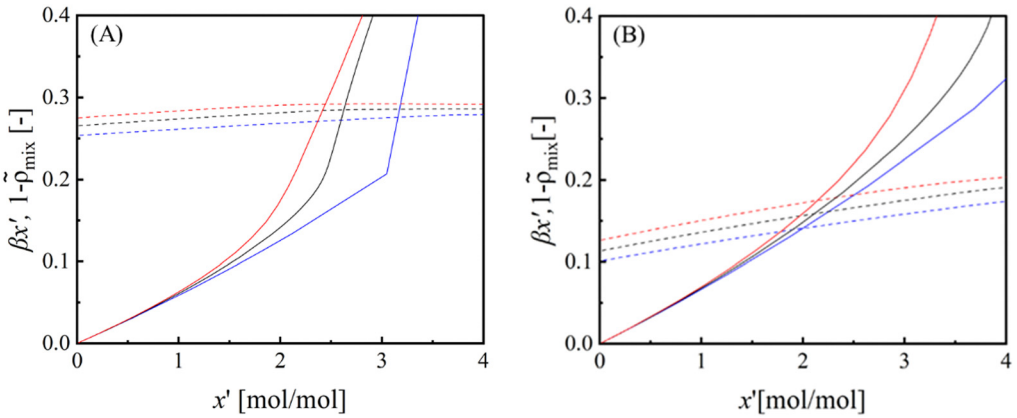

Fig. 9 Contribution of $1 - \tilde{\rho}_{mix}$ (dashed lines) and $\beta x'$ (solid lines). (A) [emim][Tf_2N] + CO_2 mixture (lines: blue, 298.15 K; black, 323.15 K; red, 343.15 K). (B): [emim][FAP] + CO_2 mixture (lines: blue, 303.15 K; black, 323.15 K; and red, 343.15 K).

mixtures, the model yielded good predictions in regions where the viscosity exceeded 10 mPa s. However, in the low-viscosity regions below 10 mPa s, the calculated values were lower than the experimental values.

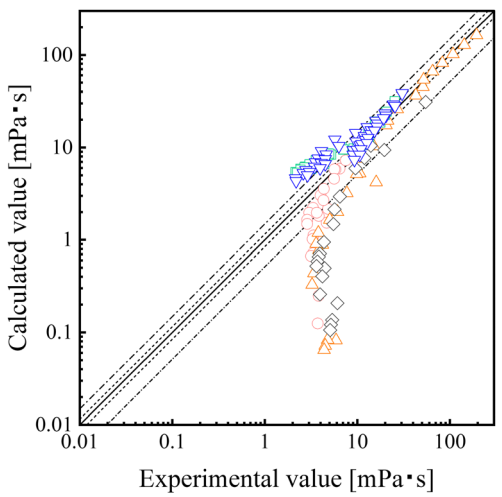

Fig. 10 Parity plot for the viscosity of the IL + CO_2 mixture (β is the value predicted by eqn (22)). Symbols: ○, [emim][Tf_2N] + CO_2 mixture;[43] Δ, [hmim][Tf_2N] + CO_2 mixture;[43] ◊, [dmim][Tf_2N] + CO_2 mixture;[43] ▽, [emim][FAP] + CO_2 mixture;[44] □, [hmim][FAP] + CO_2 mixture.[44] Dashed lines: overall ARDs (15.5% at $x' < 1.0$; see Table 6) of the FVT + ε*-mod SL-EoS. Dashed-dotted lines: overall ARDs (48.8% for the entire solubility range; see Table 6) of the FVT + ε*-mod SL-EoS.

This indicates that in low-viscosity regions with a high molar ratio of CO_2, the model based on FVT with correction by solubility parameters may have limitations in representing the viscosity of the IL + CO_2 mixtures. A more detailed evaluation is given in Table 6 and Fig. S20–S24 (ESI†), which shows that the model predicts relatively well for $x' < 1.0$. This finding indicates that the correction based on solubility parameters was excessive in the high CO_2 molar ratio region.

At present, the reason for the large differences in ARDs among the different ILs cannot be definitively identified. However, the following findings serve as important clues for identifying the possible causes of these discrepancies: (i) the deviations observed in the correlations (Table 5) are relatively small; (ii) the deviations in the solubility parameters of CO_2 are assumed to be minimal, as the parameters used in this study account for both temperature and pressure dependence; and (iii) the prediction accuracy of the densities of the IL + CO_2 systems is extremely high, as shown in Section 3.3. Taken together, these considerations indicate that the observed discrepancies are more likely due to inaccuracies in the estimated solubility parameters of the ILs or the limitations of the present approach, which rely on correcting the FVT + ε*-mod SL-EoS model based solely on solubility parameter differences. In this

Table 6 ARDs of the prediction results using β predicted by eqn (22) using solubility parameters

	ARD [%]		
Name	$x' < 1.0$	All	Ref.
[emim][Tf_2N]	6.13	36.3	43 and 44
[hmim][Tf_2N]	13.4	46.3	43 and 45
[dmim][Tf_2N]	35.3	72.9	43
[emim][FAP]	22.2	56.0	44
[hmim][FAP]	12.6	41.1	44
Overall	15.5	48.8	

study, the solubility parameters of the ILs were estimated from their critical properties for ease of calculation. However, the accuracy of this method may be limited; for example, it might cause large deviations for ILs with FAP-based anions containing a high number of fluorine atoms or fail to accurately capture subtle differences in the alkyl chain length. This aspect has room for improvement in future studies. However, this model provides a useful approach for predicting the viscosities of IL + CO_2 mixtures without the need for direct viscosity correlations by applying corrections based on the solubility parameters.

4. Conclusions

This study developed a viscosity prediction model for IL + CO_2 mixtures by combining FVT with the ε*-mod EoS. The proposed model accurately correlated the viscosities of the five imidazolium IL + CO_2 mixtures by introducing a correction term based on the molar ratio of CO_2 to IL. Furthermore, using the correction factor derived from the solubility parameters, the model enabled the prediction of the viscosity of the IL + CO_2 mixtures in regions where the molar ratio of CO_2 to IL was low ($x' < 1.0$). The introduction of solubility parameters is considered to account for the changes in the molecular structure of the ILs upon CO_2 dissolution, which cannot be fully described by FVT alone.

To enhance the versatility of the model developed in this study, further experimental data must be accumulated, and the model must be applied to these datasets. The applicability of different ILs should be verified by extending their use to a wide variety of systems, including phosphonium- and ammonium-based ILs, which were not covered in this study. To improve this model, it is important to address the limitations of this study. The increase in deviation in the high CO_2 concentration region is considered to have occurred in a region that deviates from the concept that CO_2 dissolves in the IL, increases the free volume, and weakens the ionic interactions within the ILs, thereby reducing viscosity. At high CO_2 concentrations, the interactions between CO_2 molecules should be strengthened. Therefore, representing the viscosity change in this region accurately is necessary, for example, by considering the viscosity of CO_2, although other approaches may also be possible. Alternatively, in the current model, parameters A and B, which correlate with the viscosity of pure ILs based on FVT, were also applied to the mixture system. However, for greater accuracy, these parameters must be refined to account for the mixture effects. Reassessing the contributions of the corrections used in this study is essential for evaluating the accuracy of the model. Considering the fundamental principles of this model, its applicability can extend beyond CO_2-containing systems to systems involving other gases or solvent mixtures. Therefore, future studies should explore these possibilities. Additionally, the model will be expanded to chemical absorption-type ILs by incorporating compositional changes owing to chemical absorption as variations in the free volume. Establishing such extensibility would lead to the development of a practical and widely applicable framework for predicting the viscosity of IL + CO_2 mixtures, which in turn would significantly contribute to the selection of ILs applicable to CCUS technologies.

Abbreviations

[emim] 1-Ethyl-3-methylimidazolium
[hmim] 1-Hexyl-3-methylimidazolium
[dmim] 1-Decyl-3-methylimidazolium
[Tf_2N] Bis(trifluoromethylsulfonyl)imide
[FAP] Tris(perfluoroethyl)trifluorophosphate

Author contributions

Ryohei Otani: data curation, formal analysis, software, writing, and original draft. Yuya Hiraga: investigation, methodology, software, visualization, writing – review and editing. Masaru Watanabe: conceptualization, project administration, supervision, writing – review and editing, validation, and funding acquisition.

Data availability

The data supporting this article have been included as part of the ESI.†

Conflicts of interest

There are no conflicts to declare.

Acknowledgements

This work was supported by the project JPNP18016, subsidized by the New Energy and Industrial Technology Development Organization (NEDO).

References

1 G. Li, S. Dong, P. Fu, Q. Yue, Y. Zhou and J. Wang, *Green Chem.*, 2022, **24**, 3433–3460.
2 S. N. A. Shafie, N. A. H. Md Nordin, S. M. Racha, M. R. Bilad, M. H. D. Othman, N. Misdan, J. Jaafar, Z. A. Putra and M. D. H. Wirzal, *J. Mol. Liq.*, 2022, **358**, 119192.

3 S. D. Kenarsari, D. Yang, G. Jiang, S. Zhang, J. Wang, A. G. Russell, Q. Wei and M. Fan, *RSC Adv.*, 2013, **3**, 22739.
4 J. Zhang, J. Sun, X. Zhang, Y. Zhao and S. Zhang, *Greenhouse Gases: Sci. Technol.*, 2011, **1**, 142–159.
5 K. Paduszyński and U. Domańska, *Ind. Eng. Chem. Res.*, 2012, **51**, 591–604.
6 N. Gao, Y. Yang, Z. Wang, X. Guo, S. Jiang, J. Li, Y. Hu, Z. Liu and C. Xu, *Chem. Rev.*, 2024, **124**, 27–123.
7 Z. G. Lei, C. N. Dai and B. H. Chen, *Chem. Rev.*, 2014, **114**, 1289–1326.
8 M. FitzPatrick, P. Champagne and M. F. Cunningham, *Cellulose*, 2011, **19**, 37–44.
9 M. Iguchi, K. Kasuya, Y. Sato, T. M. Aida, M. Watanabe and R. L. Smith, *Cellulose*, 2013, **20**, 1353–1367.
10 T. Numpilai, L. K. H. Pham and T. Witoon, *Ind. Eng. Chem. Res.*, 2024, **63**, 19865–19915.
11 A. Chamoun-Farah, A. N. Keller, M. Y. Balogun, L. M. Cañada, J. F. Brennecke and B. D. Freeman, *J. Membr. Sci.*, 2024, **702**, 122758.
12 E. Kamio, T. Matsuki, S. Kasahara and H. Matsuyama, *Sep. Sci. Technol.*, 2016, **52**, 209–220.
13 A. Matsuoka, A. Otani, E. Kamio and H. Matsuyama, *Sep. Purif. Technol.*, 2022, **280**, 119847.
14 L. Wang, J. Chen, S. Wang, T. Zhou, D. Li, C. Li, L. Qian, Y. Xiong, L. Miao and Z. Xie, *Sep. Purif. Technol.*, 2025, **354**, 129302.
15 X. Zhang, W. Xiong, Z. Tu, L. Peng, Y. Wu and X. Hu, *ACS Sustainable Chem. Eng.*, 2019, **7**, 10792–10799.
16 H. Kawanami, A. Sasaki, K. Matsui and Y. Ikushima, *Chem. Commun.*, 2003, 896–897.
17 P. Jaiswal and M. N. Varma, *J. CO2 Util.*, 2016, **14**, 93–97.
18 R. Macías-Salinas, *Ind. Eng. Chem. Res.*, 2024, **63**, 7387–7400.
19 Y. Sun, G. Shen, C. Held, X. Feng, X. Lu and X. Ji, *Ind. Eng. Chem. Res.*, 2018, **57**, 8784–8801.
20 A. K. Doolittle, *J. Appl. Phys.*, 1951, **22**, 1471–1475.
21 S. E. Quiñones-Cisneros, C. K. Zéberg-Mikkelsen and E. H. Stenby, *Fluid Phase Equilib.*, 2000, **169**, 249–276.
22 G. Shen, C. Held, J.-P. Mikkola, X. Lu and X. Ji, *Ind. Eng. Chem. Res.*, 2014, **53**, 20258–20268.
23 L. F. Cameretti, G. Sadowski and J. M. Mollerup, *Ind. Eng. Chem. Res.*, 2005, **44**, 3355–3362.
24 J. M. Lopes, S. Kareth, M. D. Bermejo, Á. Martín, E. Weidner and M. J. Cocero, *J. Supercrit. Fluids*, 2016, **111**, 91–96.
25 H. Machida, Y. Sato and R. L. Smith, *Fluid Phase Equilib.*, 2010, **297**, 205–209.
26 I. C. Sanchez and R. H. Lacombe, *J. Phys. Chem.*, 1976, **80**, 2352–2362.
27 I. C. Sanchez and R. H. Lacombe, *Macromolecules*, 1978, **11**, 1145–1156.
28 M. S. Shannon, J. M. Tedstone, S. P. O. Danielsen, M. S. Hindman, A. C. Irvin and J. E. Bara, *Ind. Eng. Chem. Res.*, 2012, **51**, 5565–5576.
29 W. Jeffrey Horne, M. S. Shannon and J. E. Bara, *J. Chem. Thermodyn.*, 2014, **77**, 190–196.
30 E. A. Shelepova and N. N. Medvedev, *J. Mol. Liq.*, 2022, **349**, 118127.
31 E. A. Shelepova and N. N. Medvedev, *J. Mol. Liq.*, 2022, **368**, 120740.
32 W. Beichel, Y. Yu, G. Dlubek, R. Krause-Rehberg, J. Pionteck, D. Pfefferkorn, S. Bulut, D. Bejan, C. Friedrich and I. Krossing, *Phys. Chem. Chem. Phys.*, 2013, **15**, 8821–8830.
33 G. Dlubek, Y. Yu, R. Krause-Rehberg, W. Beichel, S. Bulut, N. Pogodina, I. Krossing and C. Friedrich, *J. Chem. Phys.*, 2010, **133**, 124502.
34 Y. Yu, D. Bejan and R. Krause-Rehberg, *Fluid Phase Equilib.*, 2014, **363**, 48–54.
35 N. J. Brooks, F. Castiglione, C. M. Doherty, A. Dolan, A. J. Hill, P. A. Hunt, R. P. Matthews, M. Mauri, A. Mele, R. Simonutti, I. J. Villar-Garcia, C. C. Weber and T. Welton, *Chem. Sci.*, 2017, **8**, 6359–6374.
36 Y. Hiraga, M. Goto, Y. Sato and R. L. Smith, *J. Chem. Thermodyn.*, 2017, **104**, 73–81.
37 Y. Hiraga, K. Koyama, Y. Sato and R. L. Smith, *J. Chem. Thermodyn.*, 2017, **108**, 7–17.
38 Y. Hiraga, S. Hagiwara, Y. Sato and R. L. Smith, *J. Chem. Eng. Data*, 2018, **63**, 972–980.
39 Y. Hiraga, K. Koyama, Y. Sato and R. L. Smith, *J. Supercrit. Fluids*, 2018, **132**, 42–50.
40 Q. Guo, C. B. Park, X. Xu and J. Wang, *J. Cell. Plast.*, 2007, **43**, 69–82.
41 X. Ji, C. Held and G. Sadowski, *Fluid Phase Equilib.*, 2012, **335**, 64–73.
42 X. Y. Ji and C. Held, *Fluid Phase Equilib.*, 2016, **410**, 9–22.
43 A. Ahosseini, E. Ortega, B. Sensenich and A. M. Scurto, *Fluid Phase Equilib.*, 2009, **286**, 72–78.
44 K. Li, W. Wu, L. Peng and H. Zhang, *J. Mol. Liq.*, 2021, **337**, 116240.
45 J. J. Fillion and J. F. Brennecke, *J. Chem. Eng. Data*, 2017, **62**, 1884–1901.
46 G. Yu, D. Zhao, L. Wen, S. Yang and X. Chen, *AlChE J.*, 2011, **58**, 2885–2899.
47 X. Zhang, F. Huo, X. Liu, K. Dong, H. He, X. Yao and S. Zhang, *Ind. Eng. Chem. Res.*, 2015, **54**, 3505–3514.
48 B. F. Goodrich, J. C. de la Fuente, B. E. Gurkan, D. J. Zadigian, E. A. Price, Y. Huang and J. F. Brennecke, *Ind. Eng. Chem. Res.*, 2011, **50**, 111–118.
49 B. F. Goodrich, J. C. de la Fuente, B. E. Gurkan, Z. K. Lopez, E. A. Price, Y. Huang and J. F. Brennecke, *J. Phys. Chem. B*, 2011, **115**, 9140–9150.
50 X.-M. Zhang, K. Huang, S. Xia, Y.-L. Chen, Y.-T. Wu and X.-B. Hu, *Chem. Eng. J.*, 2015, **274**, 30–38.
51 Y. Hiraga, Y. Takikawa, M. Tatsushima and M. Watanabe, *Chem. Eng. Sci.*, 2025, **307**, 121352.
52 J. Safarov, W. A. El-Awady, A. Shahverdiyev and E. Hassel, *J. Chem. Eng. Data*, 2011, **56**, 106–112.
53 M. Iguchi, Y. Hiraga, Y. Sato, T. M. Aida, M. Watanabe and R. L. Smith, *J. Chem. Eng. Data*, 2014, **59**, 709–717.
54 R. Kato and J. Gmehling, *J. Chem. Thermodyn.*, 2005, **37**, 603–619.
55 J. Safarov, R. Hamidova, S. Zepik, H. Schmidt, I. Kul, A. Shahverdiyev and E. Hassel, *J. Mol. Liq.*, 2013, **187**, 137–156.

56 L. I. N. Tomé, P. J. Carvalho, M. G. Freire, I. M. Marrucho, I. M. A. Fonseca, A. G. M. Ferreira, J. O. A. P. Coutinho and R. L. Gardas, *J. Chem. Eng. Data*, 2008, **53**, 1914–1921.
57 D. Almantariotis, S. Stevanovic, O. Fandino, A. S. Pensado, A. A. Padua, J. Y. Coxam and M. F. Costa Gomes, *J. Phys. Chem. B*, 2012, **116**, 7728–7738.
58 K. R. Harris and M. Kanakubo, *J. Chem. Eng. Data*, 2016, **61**, 2399–2411.
59 Q. S. Liu, J. Tong, Z. C. Tan, U. Welz-Biermann and J. Z. Yang, *J. Chem. Eng. Data*, 2010, **55**, 2586–2589.
60 A. Nazet, S. Sokolov, T. Sonnleitner, T. Makino, M. Kanakubo and R. Buchner, *J. Chem. Eng. Data*, 2015, **60**, 2400–2411.
61 S. Seki, S. Tsuzuki, K. Hayamizu, Y. Umebayashi, N. Serizawa, K. Takei and H. Miyashiro, *J. Chem. Eng. Data*, 2012, **57**, 2211–2216.
62 M. Součková, J. Klomfar and J. Pátek, *J. Chem. Thermodyn.*, 2012, **48**, 267–275.
63 J.-G. Li, Y.-F. Hu, S. Ling and J.-Z. Zhang, *J. Chem. Eng. Data*, 2011, **56**, 3068–3072.
64 R. L. Gardas, M. G. Freire, P. J. Carvalho, I. M. Marrucho, I. M. A. Fonseca, A. G. M. Ferreira and J. A. P. Coutinho, *J. Chem. Eng. Data*, 2007, **52**, 1881–1888.
65 K. R. Harris and M. Kanakubo, *J. Chem. Eng. Data*, 2021, **66**, 4618–4628.
66 J. C. F. Diogo, F. J. P. Caetano, J. M. N. A. Fareleira and W. A. Wakeham, *Fluid Phase Equilib.*, 2013, **353**, 76–86.
67 M. E. Kandil, K. N. Marsh and A. R. H. Goodwin, *J. Chem. Eng. Data*, 2007, **52**, 2382–2387.
68 A. Ahosseini and A. M. Scurto, *Int. J. Thermophys.*, 2008, **29**, 1222–1243.
69 G. B. Dutt, *J. Phys. Chem. B*, 2010, **114**, 8971–8977.
70 M. Atilhan, J. Jacquemin, D. Rooney, M. Khraisheh and S. Aparicio, *Ind. Eng. Chem. Res.*, 2013, **52**, 16774–16785.
71 M. Watanabe, D. Kodama, T. Makino and M. Kanakubo, *Fluid Phase Equilib.*, 2016, **420**, 44–49.
72 T. Makino, M. Kanakubo, Y. Masuda, T. Umecky and A. Suzuki, *Fluid Phase Equilib.*, 2014, **362**, 300–306.
73 W. Ren, B. Sensenich and A. M. Scurto, *J. Chem. Thermodyn.*, 2010, **42**, 305–311.
74 E.-K. Shin, B.-C. Lee and J. S. Lim, *J. Supercrit. Fluids*, 2008, **45**, 282–292.
75 D. Almantariotis, O. Fandiño, J. Y. Coxam and M. F. Costa Gomes, *Int. J. Greenhouse Gas Control*, 2012, **10**, 329–340.
76 S. Raeissi, L. Florusse and C. J. Peters, *J. Supercrit. Fluids*, 2010, **55**, 825–832.
77 M. Gonzalez-Miquel, J. Bedia, J. Palomar and F. Rodriguez, *J. Chem. Eng. Data*, 2014, **59**, 212–217.
78 M. Althuluth, M. T. Mota-Martinez, M. C. Kroon and C. J. Peters, *J. Chem. Eng. Data*, 2012, **57**, 3422–3425.
79 A. H. Jalili, M. Shokouhi, G. Maurer and M. Hosseini-Jenab, *J. Chem. Thermodyn.*, 2013, **67**, 55–62.
80 M. Nunes da Ponte and M. E. Zakrzewska, *J. Supercrit. Fluids*, 2016, **113**, 61–65.
81 M. J. Muldoon, S. N. V. K. Aki, J. L. Anderson, J. K. Dixon and J. F. Brennecke, *J. Phys. Chem. B*, 2007, **111**, 9001–9009.
82 X. Liu, M. He, N. Lv, H. Xu and L. Bai, *J. Chem. Thermodyn.*, 2016, **97**, 48–54.
83 Z. Liu, W. Wu, B. Han, Z. Dong, G. Zhao, J. Wang, T. Jiang and G. Yang, *Chem. – Eur. J.*, 2003, **9**, 3897–3903.
84 D. Tomida, A. Kumagai, K. Qiao and C. Yokoyama, *J. Chem. Eng. Data*, 2007, **52**, 1638–1640.
85 S. N. V. K. Aki, B. R. Mellein, E. M. Saurer and J. F. Brennecke, *J. Phys. Chem. B*, 2004, **108**, 20355–20365.
86 M. Ramdin, T. W. de Loos and T. J. H. Vlugt, *Ind. Eng. Chem. Res.*, 2012, **51**, 8149–8177.
87 X. H. Huang, C. J. Margulis, Y. H. Li and B. J. Berne, *J. Am. Chem. Soc.*, 2005, **127**, 17842–17851.
88 M. Klahn and A. Seduraman, *J. Phys. Chem. B*, 2015, **119**, 10066–10078.
89 T. C. Lourenco, S. Aparicio, G. C. Costa and L. T. Costa, *J. Chem. Phys.*, 2017, **146**, 104502.
90 L. F. Lepre, M. Costa Gomes and R. A. Ando, *ChemPhysChem*, 2020, **21**, 1230–1234.
91 Y. S. Sistla and V. Sridhar, *J. Mol. Liq.*, 2021, **325**, 115162.
92 Y. Marcus, *J. Solution Chem.*, 2018, **48**, 1025–1034.
93 C. Panayiotou and V. Hatzimanikatis, *Fluid Phase Equilib.*, 2021, **527**, 112828.
94 X. Xu, H. Chen, C. Liu and C. Dang, *ACS Omega*, 2019, **4**, 13279–13294.
95 M. S. Graboski and T. E. Daubert, *Ind. Eng. Chem. Process Des. Dev.*, 1978, **17**, 448–454.
96 M. S. Graboski and T. E. Daubert, *Ind. Eng. Chem. Process Des. Dev.*, 1979, **18**, 300–306.
97 J. R. Elliott and T. E. Daubert, *Ind. Eng. Chem. Process Des. Dev.*, 1985, **24**, 743–748.
98 Y. Hiraga, W. Endo, H. Machida, Y. Sato, T. M. Aida, M. Watanabe and R. L. Smith Jr, *J. Supercrit. Fluids*, 2012, **66**, 49–58.